HTC2009

Capillary interactions between molten silicon and porous graphite

R. Israel · R. Voytovych · P. Protsenko · B. Drevet ·
D. Camel · N. Eustathopoulos

Abstract The capillary properties (wetting, infiltration) of the reactive Si/porous graphite system are studied by the sessile drop technique that enables the spreading and infiltration dynamics to be monitored in situ. The experiments are performed by varying the temperature, the type of graphite (porosity, grain size) and the vapour phase (inert gas or high vacuum). Further experiments are performed in order to quantify the influence of the exothermic reaction between Si and graphite on the temperature field close to the infiltration front. The effects of Si–graphite interactions on graphite mechanical integrity are also evidenced.

Introduction

Graphite crucibles are currently used in different stages of processing of photovoltaic silicon by metallurgical routes. Interactions between molten silicon and porous graphite, namely infiltration and reaction of formation of silicon carbide, can affect the crucible lifetime as well as silicon purity and electrical performance. Moreover reactive infiltration of silicon into carbon preforms is used to

R. Israel · R. Voytovych · N. Eustathopoulos (✉)
SIMaP/PHELMA, INPG, D.U., BP 75, 38402 St. Martin
d'Hères, France
e-mail: nikos@simap.grenoble-inp.fr

R. Israel · B. Drevet · D. Camel
CEA-INES/RDI, LITEN/DTS/LCS, 50 av. du Lac Léman,
73377 le Bourget du Lac, France

P. Protsenko
Department of Colloid Chemistry, MSU, Moscow, Russia

process the so-called "reaction bonded silicon carbide" [1–3] or SiC composites [4, 5].

The process of infiltration of Si into porous carbon preforms is generally described (see for instance [6]) as consisting of rapid, non-reactive, infiltration followed by the reaction between Si and C to form SiC. The rate of infiltration is assumed to be controlled by the viscous resistance of the liquid and the infiltration depth h varying parabolically with time t according to Washburn's equation [7]:

$$h^2 = r_{\text{eff}} \frac{\sigma \cos \theta}{2\eta} t = Kt \tag{1}$$

where σ and η are the surface tension and viscosity of the liquid, θ the equilibrium contact angle of the liquid on the solid and r_{eff} an effective pore radius characteristic of the preform [6]. The experimental results used in [6] to support the above model gave a value of the constant K that was 200 times smaller than the theoretical value K_{theor}. K_{theor} was calculated from known values of parameters σ, η and θ of pure Si and of a value r_{eff} determined experimentally from the slope of h^2 versus time straight lines obtained for various organic liquids. Einset attributed the difference between the experimental and theoretical values of K to a reduction in pore radius caused by the reaction. Note that this reduction can lead, ultimately, to a pore closure phenomenon and to infiltration interruption (see for instance [4]).

Experimental results obtained recently for the reactive infiltration of NiSi alloys into porous graphite led to a very different description of reactive infiltration [8]. Infiltration in this system does not show a parabolic trend as predicted by Washburn's equation, but is linear in time. Moreover, the activation energy of infiltration is one order of magnitude higher than the activation energy for viscous flow of

metallic melts in porous media. Therefore, it was concluded that reactive infiltration is not limited by the viscous flow but by the process at the infiltration front where the formation of the reaction product is coupled with the wetting of the pore walls by the alloy. However, the above study was for an Si alloy, not for pure Si, and the range of temperatures explored was 1170–1270 °C, i.e. much lower than the temperatures (around 1500 °C) used to study the infiltration of silicon into carbon preforms.

The aim of this investigation is to study the fundamental issues of capillary interactions between liquid Si and porous graphite with emphasis on the reactive infiltration process. New results are obtained using the sessile drop technique that enables the variation of the infiltration depth with time to be monitored in situ [8]. In addition to the infiltration data, the method provides quantitative information on wetting thus allowing the values of spreading and infiltration rates measured in the same experiment to be compared. The experiments are performed in static argon atmosphere by varying the temperature and the type of graphite, i.e. its total porosity and pore size. Specific experiments are performed in high vacuum in order to examine the role of the evaporation–condensation of Si on wetting and infiltration. Special attention is paid to studying and discussing the effect of the exothermic reaction between Si and graphite on the temperature field close to the infiltration front. For example, in [9, 10], considerable temperature increases (tens and even hundreds of degrees) close to the infiltration front were reported.

Experimental procedure

Infiltration experiments at temperatures close to the Si melting point (1412 °C) were carried out in an alumina chamber resistance heated furnace under a static atmosphere of He by the sessile drop method. The experiment consists in melting directly a piece of silicon (having a mass of about 100 mg) on the substrate and in monitoring the change in drop shape with time by a CCD camera linked to a video recorder. The video system is linked to a computer in order to monitor the time-dependent change of the contact angle θ, drop base diameter $d(t)$ and visible drop volume $V(t)$ using specific software. The infiltrated volume V_{inf} is calculated as $(V_0 - V(t))$ where V_0 is the drop volume at complete melting. In this way the height of infiltrated Si h_{Si} can be calculated, for each increment of time, by dividing V_{inf} by the contact area πR^2, where R is a drop base radius. Then the infiltration depth h is obtained by dividing h_{Si} by the volume fraction of pores α corrected to take into account the volume change due to the reaction. Details of the h_{Si} and h calculation are given in [8] where it is shown that the quantity h_{Si} can be used to determine the

general trend of the infiltration curves (linear, parabolic or other). As for the infiltration rate U_{inf}, its average value is more accurately evaluated by $U_{inf} = h_f^*/t_{inf}$, where h_f^* is the infiltration depth at the end of the experiment measured directly on metallographic sections (the symbol * is used to distinguish it from the calculated infiltration depth h).

Si of electronic purity (less than 20 ppb of total impurities) was used. Most of the experiments were performed using high-purity graphite (less than 20 ppm of impurities), provided by Carbone Lorraine Composants and referred to hereafter as 2020 graphite. For comparison purposes, a limited number of experiments were carried out using other types of graphite (Table 1). The graphite samples for the infiltration experiments were used as received, without any polishing, in order to avoid the closure of pores at the graphite surface by graphite particles formed during polishing. Before carrying out the experiments, the samples are cleaned by ultrasound in alcohol and annealed at 1430 °C for 20 min for degassing. This degassing procedure involves heating the sample in a vacuum of 10^{-6} mbar up to 1250 °C and then introducing inert gas (Ar or He) before increasing T to 1430 °C. The temperature cycle in the infiltration experiments consists in (i) heating up to 1250 °C under high vacuum followed by the introduction at this temperature of inert gas (ii) heating up to 1380 °C followed by a 10 min isothermal stage at this temperature to obtain temperature homogenisation in the furnace, (iii) heating up to the holding temperature at a rate of 20 °C/min. For holding temperatures in the range 1500–1600 °C, a high-frequency induction furnace was used. With this furnace it was possible to obtain high heating rates (100 °C/min) thereby minimising the time needed to increase the temperature from Si melting point to the holding temperature.

To measure the effect of the exothermic reaction on the specimen temperature, specific experiments were performed at two temperatures, one close to the Si melting point, and the other close to 1600 °C. For this purpose, a Pt-PtRh10% thermocouple protected by an alumina tube was introduced directly into the carbon body at a distance

Table 1 Characteristics of different types of graphite used in the present study

| | Type of graphite | | | |
	2020	6505	2450	Poco
Density ρ (g/cm³)	1.77	1.73	1.86	1.5–1.6
Pore fraction α_p	0.15	0.22	0.126	0.30
Mean pore diameter, $\bar{d}_{pores}$ (μm)	2.3	13.1	1.3	0.72
Flexural strength (MPa)	41–45	15	56	40
Roughness R_a (μm)	0.77	3.9	0.64	2.08

2020, 6505 and 2450 are from Carbone Lorraine Composants while Poco denotes the Poco AXZ-5Q
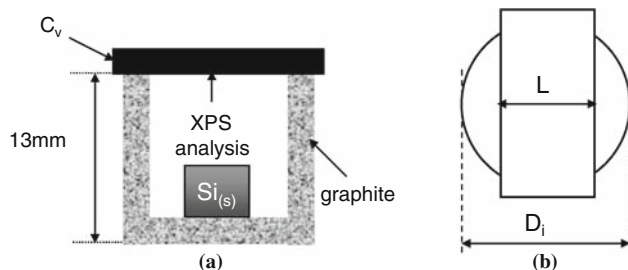
Fig. 1 Configuration used to study the evaporation–reactive condensation of Si. **a** Side view of the crucible containing a piece of Si and covered partially by a plate of vitreous carbon C_v. **b** Overhead view of the crucible and the C_v plate: the plate width L is smaller than the inner diameter D_i of the crucible

of about 2 mm from the upper surface in order to allow the infiltration front to attain the thermocouple during the process. The experiment consists in recording during the temperature rise period the difference in temperatures indicated by the above thermocouple and by a reference thermocouple situated far from the sample.

To reveal the effect of the vapour phase on the infiltration rate, a piece of Si was introduced in a graphite crucible partly covered by a vitreous carbon plate and held at 1390 °C (a temperature slightly lower than the Si melting point) for 15 min either under high vacuum (10^{-6} mbar) or in a static atmosphere of helium (Fig. 1). After the experiment, the vitreous carbon plate was transferred to an XPS chamber and the plate face exposed to Si was analysed.

Results and discussion

Wetting

Figure 2 presents an example of wetting curves (i.e. the time-dependent change in contact angle and drop base diameter) obtained during an infiltration experiment. The time origin corresponds to the beginning of melting of the droplet. Melting starts at the base of the Si sample and the solid Si/liquid Si interface moves progressively towards the top of the sample (see also Fig. 10 later on). After complete melting, spreading occurs at a nearly constant rate $U_{spr} = dR/dt$ equal to 8.7 μm/s. This is several orders of magnitude slower than the spreading rates measured previously in non-reactive liquid metal/solid systems [11–13]. In [14], on the basis of dispensed drop experiments performed in high vacuum, it was shown that the spreading rate of Si on vitreous carbon is controlled by the chemical reaction at the solid–liquid–vapour triple line where the growth of wettable SiC takes place parallel to the liquid/substrate interface (Fig. 3a, diagram). Note, however, that at temperatures close to the Si melting point, the spreading rates on polycrystalline graphite are in the range 5–10 μm/s,
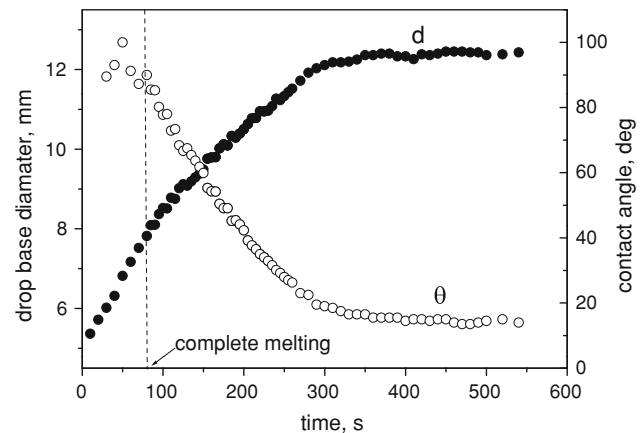

Fig. 2 Drop base diameter d and contact angle $θ$ as a function of time for Si spreading over the graphite 2020 at 1460 °C. $t = 0$ corresponds to the beginning of Si melting
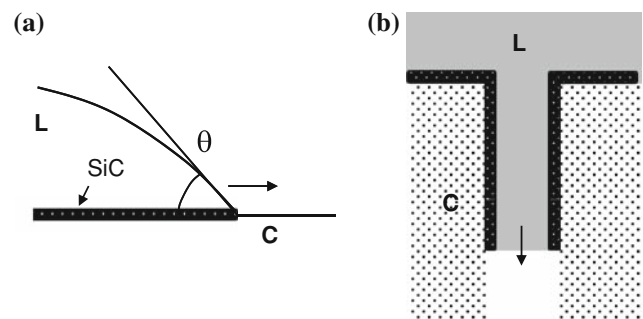

Fig. 3 Schematic presentation of reaction-controlled wetting (**a**) and infiltration (**b**) processes. Note that the scales in these two cases are very different, millimetric (**a**) and micronic (**b**)

(depending on the type of graphite, Table 2), or five times slower than U_{spr} measured by Dezellus et al. [14] on vitreous carbon. The spreading rate of reactive metal–Si alloys on vitreous carbon is higher than on polycrystalline graphite but only slightly, a few tens per cent [15, 16]. The significant difference observed in U_{spr} for pure Si on these two types of carbon is attributed to the different atmospheres used in the experiments: high vacuum in [14] compared with a static atmosphere of He in the present study. Experimental evidence for this statement will be provided in "Influence of Si transport through the vapour phase".

Infiltration

Figure 4 gives an example of the infiltration kinetics. As observed for the wetting process, infiltration of silicon is linear with time. At a time $t_{pc} ≈ 320$ s infiltration stops, thus indicating the occurrence of a *pore closure* phenomenon. The linearity of $h_{Si}(t)$ strongly suggests that infiltration is governed by the reaction of formation of SiC on the pore walls at the infiltration front (Fig. 3b). Such a

Table 2 Time needed for pore closure t_{pc} and spreading and infiltration rates for three types of graphite

Type of graphite	$\bar{d}_{pores}(\mu m)$	α_p	t_{pc} (s)	U_{inf} (μm/s)	U_{spr} (μm/s)	U_{inf}/U_{spr}
2020	2.3	0.15	∼500	5.29	5.54	0.95
2450	1.3	0.126	420	2.67	9.55	0.28
Poco	0.72	0.30	340	1.66	9.06	0.18

$T = 1430$ °C, He
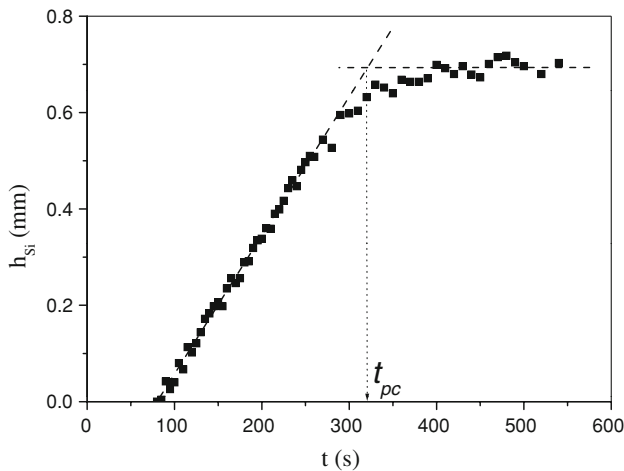
Fig. 4 Height of infiltrated Si (h_{Si}) as a function of time for an experiment performed at 1460 °C with the graphite 2020. The corresponding wetting curves are given in Fig. 2. $t = 0$ corresponds to the beginning of Si melting

Fig. 5 Arrhenius plot for infiltration rate U_{inf}

mechanism implies that the infiltration rate U_{inf} and the wetting rate U_{spr} at a given temperature are equal or at least of the same order of magnitude. This is confirmed by the experimental values of U_{inf} and U_{spr} obtained (where U_{spr} is equal to one half of the slope of $d(t)$ curves approximated by a straight line (Fig. 2)) showing that the ratio U_{inf}/U_{spr} lies between 0.18 and 0.95 depending on the type of graphite (Table 2). As argued in [8], the departure of U_{inf}/U_{spr} from unity reflects the different levels of *tortuosity* of bulk graphite and of the graphite free surface. The tortuosity is defined as the ratio between the real distance covered by a fluid between two points lying inside the porous body (or equivalently on the solid surface) and the geometrical distance between these points. In reactive infiltration the tortuosity is expected to increase when the pore size of the graphite decreases. For example, in a graphite with small pores the reaction at the infiltration front will close rapidly the smallest pores thus increasing the real distance that has to be covered by the liquid in order to advance perpendicular to the initial Si/substrate interface. This explains the low values of the ratio U_{inf}/U_{spr} observed for Poco and 2450 graphite compared to 2020.

Reaction-controlled infiltration implies a corresponding activation energy value of the order of some hundreds of
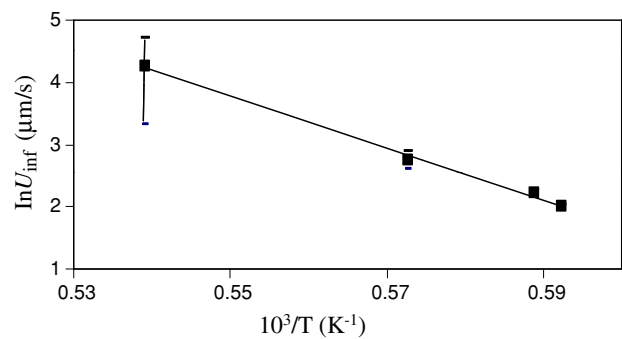
kJ/mol, as in reaction-limited wetting [17], while control by the viscous resistance of silicon would lead to a value close to the activation energy for viscous flow of silicon $E_{visc} = 30$ kJ/mol [18]. Figure 5 presents an Arrhenius plot for the U_{inf} values measured at four temperatures between 1415 and 1580 °C in the induction furnace. Due to the time δt needed to raise the temperature from Si melting point to the holding temperature, the error on the infiltration rate at the higher explored temperature (1580 °C) is high ($U_{inf} = 70 \pm 42$ μm/s). The calculated value $E_{inf} = 344 \pm 140$ kJ/mol, is one order of magnitude higher than E_{visc}.

Figure 6 gives the SEM micrograph of the infiltrated zone obtained in the experiment depicted in Figs. 2 and 4. In this experiment the total holding time at the plateau temperature was 540 s, higher than the time needed for pore closure $t_{pc} \approx 320$ s. A careful examination of the micrograph reveals the presence of a slight minimum of the infiltrated depth at the middle of the infiltration front. The minimum indicates that infiltration is interrupted first at the middle of the interface while infiltration from the periphery is still possible for a certain time. Indeed while infiltration at the centre occurs only perpendicular to the interface, at the periphery it can occur both perpendicular and parallel to this interface.

Obviously, pore closure takes place more easily for graphites that have small pores, as shown by the values of t_{pc} in Table 2. For this type of graphite, the minimum infiltration depth is particularly marked and is at the origin of the change in slope of the $h_{Si}(t)$ curve observed in this case (Fig. 7).

Fig. 6 SEM micrograph of the infiltrated zone produced in the graphite 2020 in 320 s at 1460 °C. A slight minimum in the infiltration depth h_f^* is visible in the middle of the infiltration zone
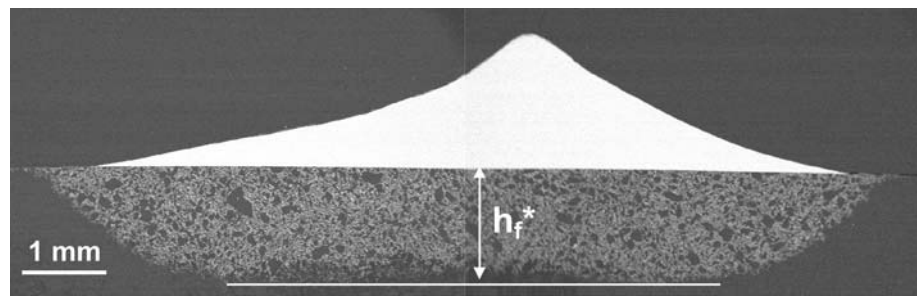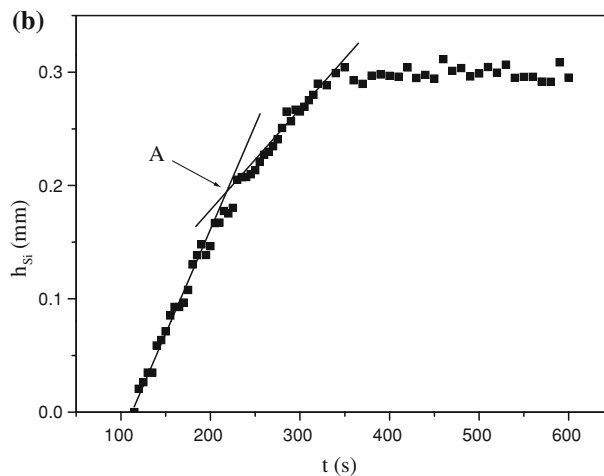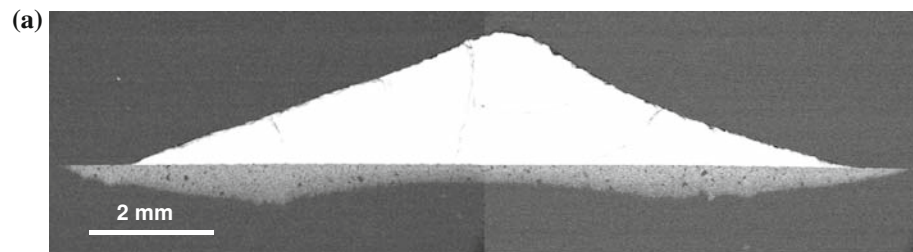

Fig. 7 a SEM micrograph of the infiltrated zone produced in the graphite Poco in 340 s at 1430 °C. **b** Height of the infiltrated Si (h_{Si}) as a function of time for this experiment. The point A corresponds to pores closure in the middle of the interface

Thermal effects during infiltration

In order to study the effect of the exothermic silicon–carbon chemical reaction on the temperature field inside the infiltrated preform, Sangsuwan et al. [9] inserted four thermocouples in a graphite preform at different distances from its lower face and, after holding the preform over an Si bath for certain time to reduce the temperature gradients, they immersed the preform in the liquid Si at 1515 °C. They observed a sharp and very strong increase in T, up to several hundred degrees, and infiltration rates 100–1000 times higher than in our experiments.

In the present study, in order to measure the temperature increase due to the reaction, three specific experiments were performed. Figure 8 presents the time-dependent change, during temperature rise to 1430 °C, of the difference, ΔT, between the temperature T_1 indicated by the
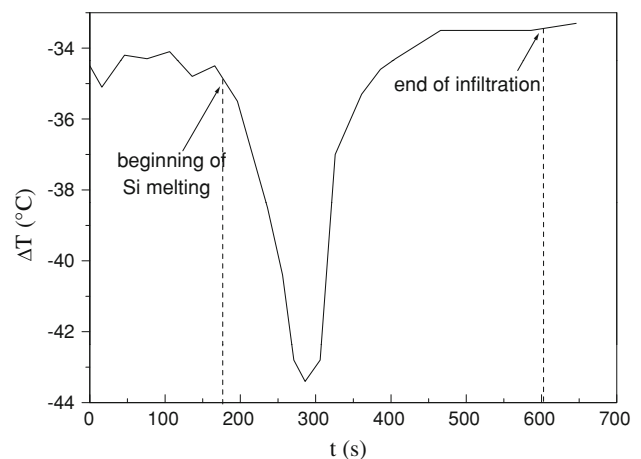

Fig. 8 Difference between the temperatures indicated by the thermocouple inserted into the graphite and a reference thermocouple during temperature rise to 1430 °C

thermocouple inserted in a 2450 graphite substrate and the temperature T_2 given by a reference thermocouple situated far from the sample. When Si starts to melt, a decrease in T_1 of up to 10 °C was detected, related to the endothermic melting of Si, whereas no measurable ΔT was found at the infiltration stage. The absence of any significant *increase* in local temperature due to the exothermic reaction was also confirmed for an experiment performed at the same temperature (1430 °C) with another type of graphite (Poco) and for an experiment carried out with graphite 2020 at 1580 °C. These results are very different from those obtained in [9] for pure Si at 1515 °C. A first reason is that the mass of Si drops used in our experiments is small compared to the mass of graphite so that the remaining unreacted graphite can chill the infiltrated region. This is different from the experiment described in [9] involving the immersion of a carbon preform in an Si bath. However, the above difference in the experimental configuration can hardly explain the differences in U_{inf} of 2–3 orders of magnitude. Second reason for this difference is that the experiment performed by Sangsuwan et al., during the time the preform was held over the liquid Si, Si atoms can diffuse inside the pore network and react with graphite to form thin SiC films on pore walls *before immersion.* If so, when the graphite preform was immersed in the molten Si, fast, viscous infiltration occurred inside the SiC-coated pores. This is a very different scenario to that of the reaction-assisted infiltration occurring in our experiments.

Experimental evidence for the effect of Si transport through the vapour phase on the wetting and infiltration processes is given in the next paragraph.

Influence of Si transport through the vapour phase

The experimental set-up schematically represented in Fig. 1 was used to check whether the transport of silicon atoms through the vapour phase can affect the surface chemistry of carbon in the case of pure Si at 1390 °C. In the first experiment, performed without Si, the XPS analysis of the C_v surface gives only the peak characteristic of pure carbon in C_v (Fig. 9). The experiment with Si in static He gives nearly the same result showing that at 1390 °C the transport of Si by diffusion in the gas is too slow to change the surface chemistry of graphite in 15 min. However, when the experiment is performed in high vacuum, where the Si transport is expected to be much faster, two changes are observed attesting the formation of a thin SiC layer a few nanometres thick on the C_v surface: first, a new peak appears at an energy characteristic of carbon in the carbide; and second, the peak of carbon in C_v is transformed into a simple shouldering. A further experiment was carried out in high vacuum at 1200 °C, a
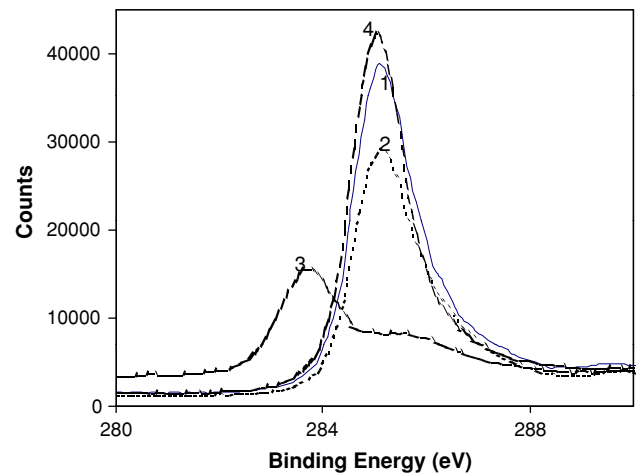

Fig. 9 XPS analysis for four C_v samples treated at different temperatures and atmospheres using the configuration shown in Fig. 1. 1: 1390 °C, He, without Si; 2: 1390 °C, He, with Si; 3: 1390 °C, vacuum, with Si; 4: 1200 °C, vacuum, with Si

temperature at which the Si partial pressure is 100 times lower than at 1390 °C. The experiment did not reveal the presence of silicon carbide on the C_v surface.

The direct influence of Si transport through the vapour phase on wetting and infiltration processes is evidenced by comparing two experiments performed with 2020 graphite (Fig. 10). In He the contact angle at melting is slightly
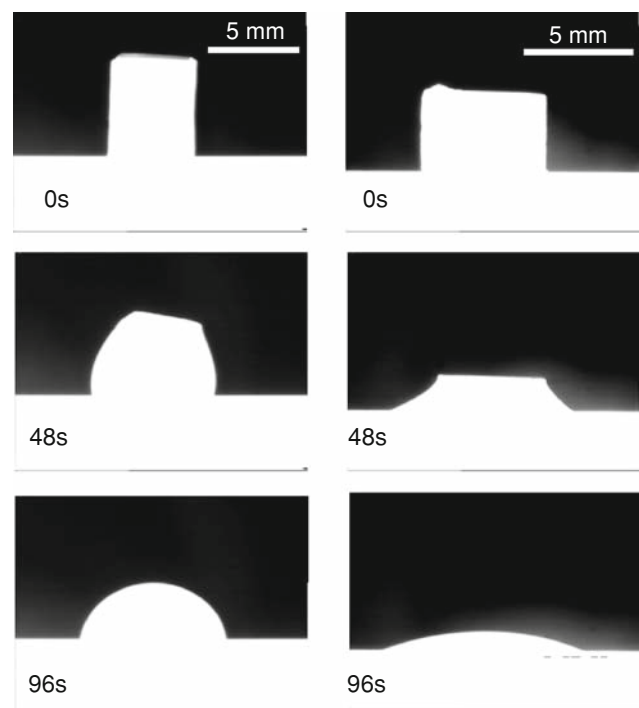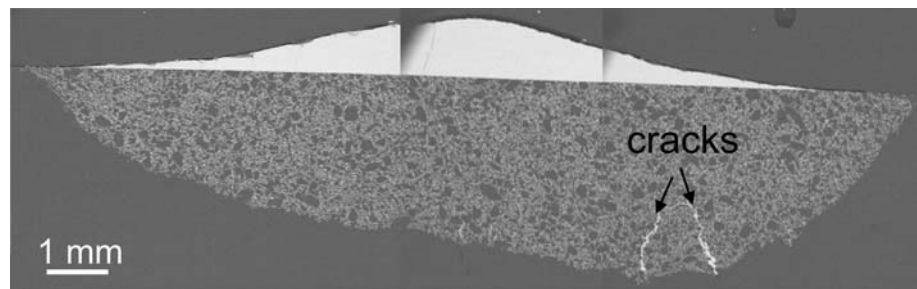

Fig. 10 Selected images of two wetting experiments performed at 1430 °C: in He atmosphere (*left*) and in vacuum (*right*). $t = 0$ corresponds to the beginning of Si melting

Fig. 11 SEM micrograph of the infiltrated zone produced in the graphite 2020 after 600 s at 1430 °C. Micro-cracks formed at the infiltration front are filled with Si

higher than 90° and decreases slowly with time as expected for a graphite sample. In contrast, in a vacuum, the contact angle formed at the beginning of melting is much lower than 90° and nearly constant with time, testifying to the presence of silicon carbide in front of the triple line. As for the infiltration rate U_{inf}, its value for infiltration under vacuum is twice as high as the value for infiltration under He.

Mechanical behaviour

The reaction of formation of SiC (molar volume $V_m = 12.5$ cm^3/mol) from graphite ($V_m = 5.5$ cm^3/mol) and silicon ($V_m = 11.6$ cm^3/mol) is accompanied by volume change which creates stress leading to crack formation during infiltration. This is responsible for the dissymmetric infiltration zone observed in the micrograph of Fig. 11. Cracking is rare with the graphites 2020, 2450 and Poco but it is very pronounced with low-strength graphite such as 6505 (Table 1). With this graphite, after 3 min of infiltration, an enhancement in the infiltration rate was observed followed by the sudden disappearance of the drop

from the field of vision. After the experiment the graphite was found to be completely broken (Fig. 12).

Conclusions

Infiltration of porous graphite by molten silicon in the temperature range 1415–1580 °C under inert gas is governed by the reaction of formation of wettable SiC on the pore walls at the infiltration front. The infiltration rate is constant with time and has an activation energy of 344 ± 140 kJ/mol. The type of graphite influences the infiltration rate mainly by its tortuosity, a parameter which depends critically on the pore size. The pore size also determines the time required for pore closure (and thus the maximum infiltration depth) caused by the reaction. In high vacuum the transport of Si atoms through the vapour phase can modify the surface chemistry of graphite in front of the triple line and thus enhance wetting and infiltration rates even at temperatures close to the Si melting point. A similar effect is expected to occur under inert gas but at much higher temperatures. Stress generated by the reaction during infiltration can cause crack formation close to the infiltration front leading ultimately to fracture of the graphite.
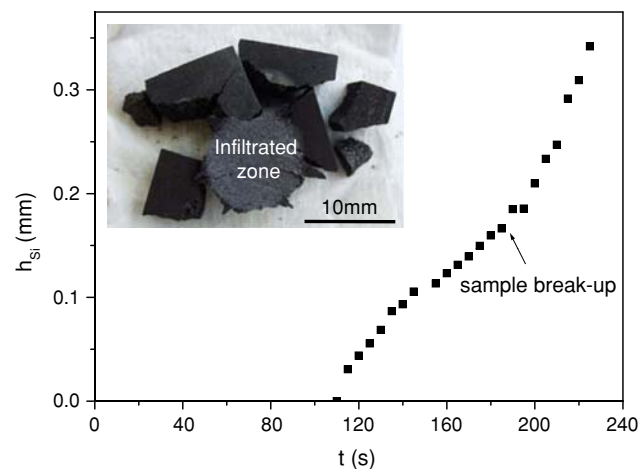

Fig. 12 Height of the infiltrated Si (h_{Si}) as a function of time for an experiment performed at 1430 °C with the graphite 6505. $t = 0$ corresponds to the beginning of Si melting. Inserted is a photo of the sample after experiment

References

1. Wang Y, Tan S, Jiang D (2004) Carbon 42:1833
2. Forrest CW, Kennedy P, Shennan JV (1972) In: Popper P (ed) Special ceramics, vol 5. British Ceramic Research Association, Stroke-on-Trent
3. Ness JN, Page TF (1986) J Mater Sci 21:1377. doi:10.1007/BF00553278
4. Messner R, Chiang YM (1990) J Am Ceram Soc 73:1193
5. Hozer L, Lee JR, Chiang YM (1995) Mater Sci Eng A 195A:131
6. Einset EO (1996) J Am Ceram Soc 79:333
7. Washburn EW (1921) Am Phys Soc 17:374
8. Voytovych R, Bougiouri V, Calderon NR, Narciso J, Eustathopoulos N (2008) Acta Mater 56:2237
9. Sangsuwan P, Tewari NS, Gatica JE, Singh M, Dickerson R (1999) Metall Mater Trans 30:933
10. Einset EO (1998) Chem Eng 53:1027
11. Eustathopoulos N, Nicholas M, Drevet B (1999) Wettability at high temperature. Pergamon Materials Series: vol 3. Pergamon, Oxford

12. Saiz E, Tomsia AP (2004) Nat Mater 3:903
13. Protsenko P, Kozlova O, Voytovych R, Eustathopoulos N (2008) J Mater Sci 43:5669. doi:10.1007/s10853-008-2814-8
14. Dezellus O, Jaques S, Hodaj F, Eustathopoulos N (2005) J Mater Sci 40:2307. doi:10.1007/s10853-005-1950-7
15. Dezellus (2000) PhD Thesis, INP Grenoble
16. Rojo-Calderon N (2009) PhD Thesis, University of Alicante
17. Bougiouri V, Voytovych R, Dezellus O, Eustathopoulos N (2007) J Mater Sci 42:2016. doi:10.1007/s10853-006-1483-8
18. Battezzati L, Greer AL (1989) Acta Metall 37:1791